Inorganic Chemistry
Article
pubs.acs.org/IC

Oligonuclear Fe Complexes (Fe, Fe_4, Fe_6, Fe_9) Derived from Tritopic Pyridine Bis-Hydrazone Ligands—Structural, Magnetic, and Mössbauer Studies

Muhammad U. Anwar,[†] Louise N. Dawe,[‡] Stewart R. Parsons,[†] Santokh S. Tandon,[§] Laurence K. Thompson,*[,†] Subrata K. Dey,[†] Valeriu Mereacre,[∥] William M. Reiff,[⊥] and Scott D. Bunge[#]

[†]Department of Chemistry, Memorial University, St. John's, Newfoundland A1B3X7, Canada
[‡]Department of Chemistry, Wilfrid Laurier University, Waterloo, Ontario N2L 3C5, Canada
[§]Department of Chemistry, Kent State University—Salem, Salem, Ohio 44460, United States
[∥]Department of Chemistry, Karlsruhe Institute of Technology, Karlsruhe, Germany
[⊥]Department of Chemistry, Northeastern University, Boston, Massachusetts 02115, United States
[#]Department of Chemistry, Kent State University, Kent, Ohio 44242, United States

Supporting Information

ABSTRACT: Tri-topic pyridine bis-hydrazone ligands produce polynuclear complexes with Fe(II) and Fe(III) salts with varying nuclearity and metal ion oxidation states. Mononuclear, tetranuclear, hexanuclear, and nonanuclear examples are discussed using structural, magnetic and Mössbauer data. In one case, although X-ray data suggest a [3 × 3] Fe_9 grid (space group $P4_2/n$), careful examination of the structure, in conjunction with magnetic and Mössbauer data, indicates an unusual situation where the corner and center sites are present at unit occupancy, whereas side site occupancy is ~0.6.

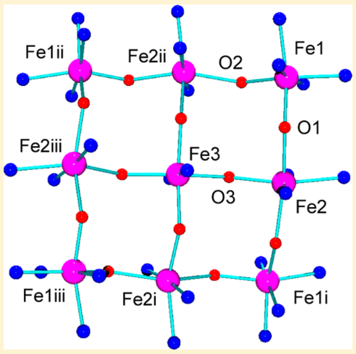

INTRODUCTION

Poly-*n*-topic ligands with appropriately chosen coordination pockets (*n*), arranged in such a way as to bind linear arrays of metal ions, have the potential to organize a much larger number of metal ions (n^2) through programmed self-assembly in the formation of [*n* × *n*] square grids. This has been achieved with a series of "linear" polytopic heterocyclic hydrazone ligands. Ditopic (e.g., poap; *n* = 2) and tritopic (e.g., 2poap and analogues; *n* = 3) pyridine based ligands and tetratopic extended pyridazine (e.g., L1, L2; *n* = 4) and pyrimidine hydrazone based ligands (e.g., L3; *n* = 4) (Chart 1) have led to the synthesis of a large number of square [*n* × *n*] polymetallic transition metal grids with, e.g., Mn(II), Co(II), Ni(II), and Cu(II).[1−3] Scheme 1 illustrates a generalized self-assembly process for a [3 × 3] example. Other classes of polytopic ligands include heterocyclic extended pyridyl-pyrimidines and pyridyl-bipyridazines, which have led to examples of M_4 [2 × 2] (Fe(II), Co(II), Zn(II)),[4] M_9 [3 × 3] (Ag(I)),[5] and M_{16} [4 × 4] (Pb(II))[6,7] square grids. A larger pentatopic pyridazine ligand was reported by Lehn et al. but did not produce the expected [5 × 5] grid, forming instead an icosanuclear $Ag(I)_{20}$ partial grid.[8] However, in the case of the pentatopic extended 2,6-bis-pyridyl-hydrazone ligand L4, indirect evidence for a [5 × 5] square Mn_{25} grid was obtained from CITS (Current Imaging Tunneling Spectroscopy), which clearly showed the presence of 25 Mn centers in the expected grid arrangement.[9]

The "tritopic" 2,6-picolinic-bis-hydrazone ligands (e.g., 2poap and analogues; Chart 1) form [3 × 3] self-assembled M_9 (M = Mn(II), Cu(II), Zn(II)) grids, in high yield.[10−14] $[Mn_9(2poap)_6]$ $(ClO_4)_6$ (Figure 1; Chart 1) is a typical example, with the nine metal ions held in a [3 × 3] grid array within the assembly of six ligands. The Mn(II) centers are antiferromagnetically coupled, due to superexchange through the 12 hydrazone oxygen bridges, resulting in a ground state spin of $S' = 5/2$. Mn(II) and Zn(II) have zero crystal field stabilization (CFS) demands and so do not have a significant preference for a particular coordination environment, and in essence the programmed instructions in the ligand topology are the controlling element in the self-assembly process. The appropriate coordination pocket donor content and the linear disposition of the pockets lead to the square [*n* × *n*] grid as the preferred oligonuclear outcome. Cu(II) has a low CFS demand, and so there is only a minor CFS based control. $Cu(II)_9$ [3 × 3] grids are common. One $Co(II)_9$ [3 × 3] grid has been reported,[3b,c] but thus far no genuine [3 × 3] $Ni(II)_9$ grids have

Received: February 12, 2014
Published: April 24, 2014

Chart 1. Polytopic Hydrazone Ligands

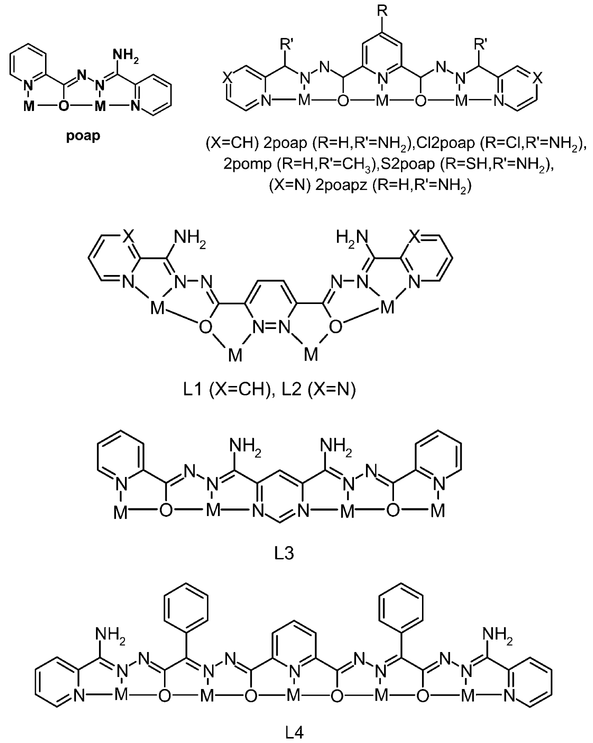

Scheme 1. Self-assembly Process for the Formation of a [3 × 3] M$_9$ Grid

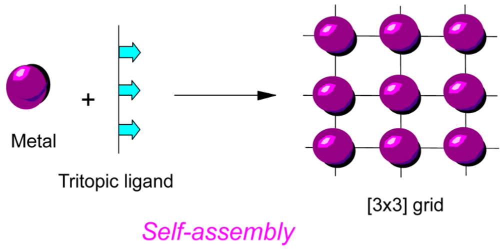

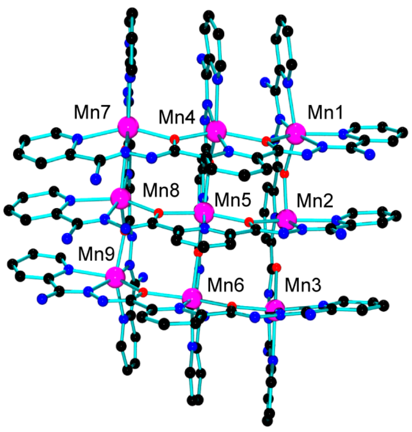

Figure 1. Structural representation of the Mn$_9$ grid cation in [Mn$_9$(2poap)$_6$](ClO$_4$)$_6$.

been produced with tritopic hydrazone ligands in this class. Partial grids form for the most part,[14] with examples of hexanuclear Ni(II) and heptanuclear Co(II)/Co(III) examples, having incomplete grid structures with five ligands instead of six and remote pairs of linear Ni(II)$_3$ groups (Ni$_6$) and two remote linear Co$_3$ groups with a single intervening cobalt ion (Co$_7$). Oxidation in the case of cobalt occurs spontaneously in the presence of air to produce mixed valence species.[15] The higher CFS demands of Co(II) and Ni(II), and the reduced bond lengths associated with Co(III) centers, clearly influence the self-assembly process, and competing coordination assemblies seem to interfere with the expected [3 × 3] grid formation.

Some Mn(II)$_9$ [3 × 3] grids exhibit unprecedented redox properties, with an eight electron reversible redox window between 0.5 and 1.6 V (vs Ag/AgCl),[10,11,13] associated with the oxidation of the eight Mn(II) centers in the outer ring of the grid to Mn(III). Selective oxidation of just the corner Mn(II) centers can be readily achieved using electrochemical methods, and by using simple chemical oxidants, e.g., Cl$_2$, OCl$^-$, and [Mn(II)$_5$Mn(III)$_4$], [3 × 3] square grids can be isolated as air stable dark brown crystalline solids.[10] The magnetic properties of the Mn grids are dominated by antiferromagnetic exchange and are modulated when oxidation occurs, leading to controlled changes in the ground state spin from $S' = 5/2$ in the Mn(II)$_9$ case to $S' = 1/2$ in the [Mn(II)$_5$Mn(III)$_4$] case.[10,14] Suitably modified Mn$_9$ grids with sulfur and chlorine appended ligands (Chart 1; e.g., S2poap, Cl2poap) adhere to Au(111) surfaces and also form SAMS (self-assembled monolayers), as shown by STM (Scanning Tunneling Microscopy) measurements.[10,16] The flat molecular orientations on the surface are associated with the prominent external positions of the sulfur and chlorine sites on the grid extremities, which provide convenient gold surface atom contacts. Ordered arrays of functionally active molecules of this sort are considered important targets for nanoscale device assemblies.[17−20]

Surface studies on [Mn$_9$(Cl2poap)$_6$](ClO$_4$)$_6$ deposited on HOPG (highly ordered pyrolytic graphite) have also been carried out and reveal not only the individual grid cations in STM topography but also the spatial arrangement of the individual metal centers using the CITS (Current Imaging Tunneling Spectroscopy) imaging technique.[13] This powerful surface structural approach probes the density of states close to the Fermi level of the system and allows discrimination between metal "3d" based HOMO (highest occupied molecular orbital) levels and ligand orbitals, which occur at quite different energies, and consequently clearly reveals the metal ion positions. Grid core dimensions obtained by this method closely match those revealed by single crystal structural methods, even to the details of the canted sideways orientation of the grid on the surface. Similar observations have recently been made with a Co(II)$_4$ [2 × 2] square grid system,[17] a Cu(II)$_{20}$ wheel shaped polyanion,[18] and a Fe(III)$_4$ star shaped cluster.[19] The importance of these techniques for addressing and probing metal centers in supramolecular assemblies applied to surfaces is discussed in more detail in a review article.[20]

Fe(II) is close to Mn(II) in its CFS demand and is also subject to oxidation, mostly on exposure to air. [3 × 3] Fe$_9$ grid structures have not yet been reported but have the potential to exhibit interesting magnetic and redox properties. In the present study, a series of oligonuclear Fe complexes of three closely related tritopic 2,6-bis-picolinic hydrazone ligands (2poap, 2poapz, Cl2poap; Chart 1) is described, with mononuclear, tetranuclear, hexanuclear, and nonanuclear examples. In addition, mixed oxidation state, Fe(II)/Fe(III), [3 × 3] grid based species are described, which exhibit unusual structural and magnetic properties and have partial occupancies at some Fe(II) sites. Structural, magnetic, and Mössbauer data are presented and discussed.

Table 1. Crystallographic Details for Complexes 1–3, 4a, 5

	1	2	3
chemical formula	$C_{17}H_{25}FeN_{14}O_{16}$	$C_{68}H_{90}Fe_4N_{50}O_{43}$	$C_{126}H_{122}Cl_8Fe_9N_{60}O_{51}$
M	737.32	2519.16	4078.97
T (K)	153(2)	163(2)	163(2)
cryst syst	monoclinic	triclinic	triclinic
space group	$C2/c$ (#15)	$P\bar{1}$ (#2)	$P\bar{1}$ (#2)
a (Å)	14.157(3)	14.236(6)	18.125(8)
b (Å)	21.058(4)	17.624(8)	18.678(8)
c (Å)	11.798(3)	22.090(9)	25.9906(10)
α (deg)	90	103.086(5)	79.350(11)
β (deg)	121.286(4)	99.396(6)	85.305(17)
γ (deg)	90	101.103(2)	89.546(15)
V (Å^3)	3005.8(11)	5172(4)	8618(5)
Z	4	2	2
D_{calc} (g/cm^3)	1.629	1.618	1.572
μ (Mo Kα) (mm^{-1})	0.598	0.664	0.955
reflns total	19 492	44 744	70 475
reflns unique ($I > 2.00\sigma(I)$)	3120 (3073)	21287 (16076)	31770 (22779)
R_{int}	0.0368	0.0497	0.0569
R_1 ($I > 2.00\sigma(I)$)	0.0671	0.1140	0.1200
wR_2 (all reflections)	0.1946	0.3775	0.3834

	4a	5
chemical formula	$C_{128}H_{117.5}Cl_{14}Fe_{6.86}N_{58.5}O_{49}$	$C_{103}H_{115}Cl_{13}Fe_6N_{46}O_{57}$
M	4138.65	3705.36
T (K)	153(2)	100(2)
cryst syst	tetragonal	triclinic
space group	$P4_2/n$ (#86)	$P\bar{1}$ (#2)
a (Å)	20.116(2)	16.2650(14)
b (Å)	20.116(2)	22.783(2)
c (Å)	21.630(2)	24.766(2)
α (deg)	90	71.147(2)
β (deg)	90	76.986(2)
γ (deg)	90	87.887(2)
V (Å^3)	8752(2)	8455.4(13)
Z	2	2
D_{calc} (g/cm^3)	1.570	1.455
μ (Mo Kα) (mm^{-1})	0.862	0.799
reflns total	68 990	68 754
reflns unique ($I > 2.00\sigma(I)$)	7707 (7424)	29884 (17897)
R_{int}	0.0420	0.0528
R_1 ($I > 2.00\sigma(I)$)	0.0972	0.0463
wR_2 (all reflections)	0.2834	0.1636

■ EXPERIMENTAL SECTION

Variable temperature DC and AC magnetic measurements were carried out using a Quantum Design MPMS5S SQUID magnetometer (0–5 T), with diamagnetic corrections applied using Pascal's constants and appropriate corrections for sample holders used. Elemental analyses were carried out by Canadian Microanalytical, Delta, BC. The complexes are listed with the formulas based on the elemental analysis and may differ from those obtained through the structural analysis. Magnetic calculations were based on molar masses obtained from the elemental analysis data.

The Mössbauer spectra on **4c** were recorded using a conventional spectrometer in the constant acceleration mode equipped with a ^{57}Co source (3.7 GBq) in a rhodium matrix. Isomer shifts are given relative to α-Fe at room temperature. The sample was inserted inside an Oxford Instruments Mössbauer-Spectromag 4000 Cryostat.

Single Crystal X-Ray Diffraction Studies. The diffraction intensities of **1**, **2**, **3**, **4a**, and **4c** were collected on a Rigaku Saturn CCD area detector equipped with a SHINE optic, with Mo Kα radiation. For **5**, the diffraction intensities were collected with graphite-monochromatized Mo Kα X-radiation λ = 0.71073 Å (Bede Microsource) using a Bruker Proteum M diffractometer, while for **4b**, the diffraction intensities were collected with graphite-monochromatized Mo Kα X-radiation using a Bruker P4 diffractometer. For both **4b** and **5**, data processing was carried out using the SAINT[21] and XPREP[22] software packages with absorption corrections applied using SADABS.[23] All data were corrected for Lorentz and polarization effects. Structures were solved by direct methods[24] and expanded using Fourier techniques.[25] Hydrogen atoms were introduced in calculated positions and refined on the riding model. All other atoms were refined anisotropically. Neutral atom scattering factors and anomalous dispersion effects were taken from the usual sources.[26−29] All calculations were performed using the CrystalStructure[30,31] (**1**, **2**, **3**), OLEX2[32] (**4a–c**), or SHELXTL[33] (**5**) crystallographic software packages except for refinement, which was performed using SHELX.[22]

In **1**, protons on the 1.5 lattice water molecules O(8, 9) could not be located in difference map positions and hence were omitted from the model; they were included in the formula for the calculation of intensive properties. In **2**, the nitrate anions were treated with similarity restraints. While H8, H19, H30, and H41 were introduced in calculated positions, they were first located in difference map positions to confirm their presence as they were required for charge balance. In **3**, the H atoms on lattice solvent water molecules could not be located from difference maps and were therefore omitted from the model but included in the formula for the calculation of intensive properties. Similarity, distance, and angle restraints were applied to several lattice solvent acetonitrile molecules and one disordered perchlorate.

For **4a**, similarity and isotropic restraints were required in the modeling of disordered lattice solvent molecules and a disordered perchlorate anion. Charge balance was not achieved due to the presence of a partial occupancy iron site in the core structure. Fe2 refined with an occupancy of 0.464(4), which led to difficulty in locating the requisite partial anionic charges in the disordered lattice solvent region.

For **5** and **4c**, the Platon[34] SQUEEZE procedure was applied. For **5**, a potential solvent volume of 4312.5 Å^3 with an electron count of 1427 electrons per cell was identified. This is consistent with 16 perchlorate, 12 methanol, two acetonitrile, and 18 water molecules per cell. The molecules omitted by SQUEEZE were included in the formula for the calculation of intensive properties. For **4c**, 720 electrons per unit cell were recovered in one void (total volume 3111 Å^3); that is 360 electrons per formula unit. For **4b**, the OLEX2[32] solving masking procedure was applied to recover 590 electrons per unit cell in one void (total volume 2772.8 Å^3); that is 295 electrons per formula unit. For **4b** and **4c**, the application of a solvent mask gave a significant improvement in the data statistics; however, charge balance was not achieved. Problems arose in that the site identified as Fe2 refined to an occupancy of 0.602(4) in **4b** and 0.617(3) in **4c**. For **4b** and **4c**, the electrons found in the void region have not been assigned and have not been included in the formula. The reported values for the intensive properties of this complex (i.e., molecular weight, density, etc.) are therefore lower than the real values. It is likely that the missing anionic charge was present in the disordered region of the structure.

CCDC #984008−984014 are for **1**−**3**, **4a**−**4c**, and **5**, respectively. Please see Table 1 for a summary of the data collection conditions and refinement results for compounds **1**−**3**, **4a**, and **5**. See the Supporting Information for crystallographic details for **4b** and **4c**.

Synthesis of Complexes. *[(2poapz)Fe(H$_2$O)$_2$(NO$_3$)](NO$_3$)$_2$·2H$_2$O (**1**), [(2poapz-H)$_4$Fe$_4$](NO$_3$)$_6$·9H$_2$O (**2**).* 2poapz[35] (0.060 g, 0.15 mmol) was added to a solution of Fe(NO$_3$)$_3$·9H$_2$O (0.20 g, 0.50 mmol) in MeOH/CH$_3$CN/H$_2$O (10 mL/10 mL/5 mL), and the mixture was stirred at 60 °C for 40 min. The volume of the resulting bluish green solution was reduced to 10 mL on the hot plate and left at room temperature for slow evaporation. A small quantity (∼10 mg) of red crystals of **1** formed after 3 weeks, which were characterized by an X-ray structural determination only. The reaction was repeated under slightly different conditions. 2poapz (0.050 g, 0.13 mmol) was added to a solution of Fe(NO$_3$)$_3$·9H$_2$O (0.20 g, 0.50 mmol) in MeOH/CH$_3$CN/H$_2$O (5 mL/5 mL/5 mL), and the mixture was stirred at room temperature for 20 min and filtered. Dark, almost black crystals of **2** separated after several weeks (yield 35 mg, 11%), suitable for structural determination. Elem. Anal. Calcd for (C$_{17}$H$_{14}$N$_{11}$O$_2$)$_4$Fe$_4$(NO$_3$)$_6$(H$_2$O)$_9$: C, 34.43; H, 2.95; N, 29.53. Found: C, 34.40; H, 2.60; N, 29.58.

*[(2poap)$_6$Fe$_9$](ClO$_4$)$_8$·18H$_2$O (**3**).* Fe(ClO$_4$)$_2$·6H$_2$O (0.12 g, 0.31 mmol) and 2poap[3a] (0.15 g, 0.34 mmol) were added to degassed MeCN (5 mL), and the mixture was stirred under a nitrogen atmosphere for 45 min at room temperature. The dark, almost black solution was set aside, sealed, and left undisturbed at room temperature. Dark green black crystals suitable for a structural determination formed after several days and were separated quickly to avoid exposure to air (yield 35 mg, 18%). Elem. Anal. Calcd for (C$_{19}$H$_{15}$N$_9$O$_2$)$_6$Fe$_9$(ClO$_4$)$_8$(H$_2$O)$_{18}$: C, 33.97; H, 3.15; N, 18.76; Fe, 12.47. Found: C, 33.94; H, 2.26; N, 18.85; Fe, 11.90. The bulk sample appears to have lost acetonitrile and become hydrated on standing.

*[(Cl2poap)$_6$Fe$_7$](ClO$_4$)$_8$·15H$_2$O (**4a**).* Fe(ClO$_4$)$_2$·6H$_2$O (0.70 g, 1.9 mmol) was dissolved in a mixture of dry MeOH/MeCN (50/50; 50 mL) in a N$_2$ atmosphere. Cl2poap[11] (0.44 g, 1.0 mmol) was added and the mixture refluxed for 24 h under N$_2$. The resulting dark solution was filtered and crystallization induced by ether diffusion to give a dark, almost black crystalline solid (yield 0.30 g, 33%). The complex was recrystallized from MeCN solution by ether diffusion to give black prisms suitable for structural study. Elem. Anal. Calcd for (C$_{19}$H$_{14}$N$_9$O$_2$Cl)$_6$Fe$_7$(ClO$_4$)$_8$(H$_2$O)$_{15}$: C, 33.63; H, 2.82; N, 18.57. Found: C, 33.71; H, 2.29; N, 18.42.

*[(Cl2poap)$_6$Fe$_{7.5}$](ClO$_4$)$_8$·14H$_2$O (**4b**).* Cl2poap[11] (0.80 g, 1.8 mmol) was suspended in degassed acetonitrile (10 mL) with stirring in a N$_2$ atmosphere. Fe(ClO$_4$)$_2$·6H$_2$O (2.8 g, 7.6 mmol) and metallic iron powder (0.45 g, 8.1 mmol) were mixed in a second flask in acetonitrile (100 mL) with stirring under N$_2$ at room temperature. The resulting colorless solution of iron(II) was filtered through a glass U-tube (to eliminate excess Fe(s)) into the flask containing the ligand. A very dark red solution formed immediately, which was heated to roughly 80 °C with stirring for 2 h and then stirred overnight at room temperature. The solution volume was reduced to roughly 25 mL under a vacuum and 4 mL of chloroform added under N$_2$. Very dark, almost black crystals formed after a week, which were collected by suction filtration and washed with a small amount of ice-cold 50/50 acetonitrile/chloroform solution (yield = 0.90 g; 67%). A portion of the initial crystalline product was recrystallized by ether diffusion into a solution in a methanol/acetonitrile mixture without excluding air and obtained as dark almost black crystals of **4b**, suitable for structural determination. Anal. Calcd for [(C$_{19}$H$_{14}$N$_9$O$_2$Cl)$_6$Fe$_{7.5}$](ClO$_4$)$_8$·14H$_2$O: C, 33.55; H, 2.77; N, 18.53; Cl, 12.16. Found: C, 33.71; H, 2.29; N, 18.42; Cl, 11.45. MALDI/TOFMS: 3208.9 ([L$_6$Fe$_9$](ClO$_4$)$^+$), 3157.0, ([L$_6$Fe$_8$](ClO$_4$)$^+$), 3110.9 (s) ([L$_6$Fe$_9$]$^+$), 3056.2 (ms) ([L$_6$Fe$_8$]$^+$), 3001.4 (w) ([L$_6$Fe$_7$]$^+$). The presence of peaks associated with depleted Fe grids, but still with six ligands, supports the suggestion of a mixture of grids with different Fe content. The estimated relative intensities for the grid peaks (100%, 55%, 10% respectively) suggest that the fully metalated grid is the dominant component, but only for +1 charged ions. Other charged ions corresponding to grid species would probably reflect a differing distribution of occupancies.

*[(Cl2poap)$_6$Fe$_{7.4}$](ClO$_4$)$_8$·22H$_2$O (**4c**).* Fe(ClO$_4$)$_2$·6H$_2$O (1.25 g, 3.44 mmol) was dissolved in MeCN (30 mL) under N$_2$ and 0.12 g of ascorbic acid added, and the mixture was stirred at RT for 15 min. Cl2poap[11] (0.5 g, 1.14 mmol) was added, and the mixture was stirred under a nitrogen atmosphere for 6 h. The dark, almost black, solution was reduced in volume under reduced pressure to 10 mL and filtered in the air. Dark green almost black crystals formed on prolonged standing, suitable for structural determination (yield 0.32 g, 42%). Elem. Anal. Calcd for (C$_{19}$H$_{14}$N$_9$O$_2$Cl)$_6$Fe$_{7.4}$(ClO$_4$)$_8$(H$_2$O)$_{22}$: C, 32.45; H, 2.82; N, 17.93: Cl, 11.76; Fe, 9.79. Found: C, 32.62; H, 2.35; N, 18.08; Cl, 12.17, Fe, 9.59.

*[(Cl2poap)$_5$Fe$_6$](ClO$_4$)$_8$·20H$_2$O (**5**).* In a synthesis similar to that of **4a**, but using somewhat milder reaction conditions, crystals of a hexanuclear complex (**5**) were isolated from the mother liquor, which differed structurally from **4a**, giving some insight into the intermediates which might be involved in the synthesis of a complete grid.

Cl2poap[11] (0.22 g, 0.50 mmol) was added to a solution of Fe(ClO$_4$)$_2$·6H$_2$O (0.73 g, 2.0 mmol) dissolved in degassed CH$_3$CN (30 mL) under an atmosphere of nitrogen gas. The reaction mixture was stirred at ∼60 °C for 4 h, then left at room temperature overnight. The initially deep red solution changed in color to dark greenish brown on heating. The volume of the solution was reduced to 10 mL under reduced pressure and CHCl$_3$ (3 mL) adder under nitrogen. A dark greenish brown solid separated on standing (∼50 mg), which was separated by filtration, washed with MeOH, and dried. Variable temperature magnetic data on this sample were very similar to those observed for **4a**−**4c** (*vide infra*), suggesting a similar [3 × 3] grid. This material was not examined further. The mother liquor was left to evaporate slowly at room temperature and produced large dark green crystals suitable for structural determination (yield 80 mg, 22%). Elem. Anal. Calcd for (C$_{19}$H$_{14}$N$_9$O$_2$Cl)$_5$Fe$_6$(ClO$_4$)$_8$(H$_2$O)$_{20}$: C, 31.09; H, 3.02; N, 17.17. Found: C, 31.05; H, 2.40; N, 16.88.

Description of the Structures. *[(2poapz)Fe(H$_2$O)$_2$(NO$_3$)](NO$_3$)$_2$·2H$_2$O (**1**).* The molecular structure of **1** is shown in Figure 2. Crystallographic details are given in Table 1 and important distances and angles in Table 2. The structure is mononuclear with the ligand

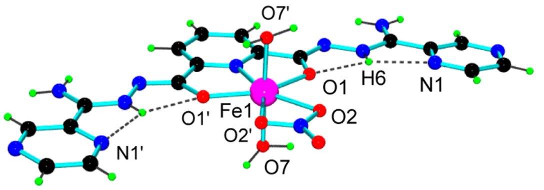

Figure 2. Structural representation of the cation in $[(2poapz)Fe(H_2O)_2(NO_3)](NO_3)_2\cdot 2H_2O$ (**1**).

Table 2. Selected Distances (Å) and Angles (deg) for 1 (Symmetry Operator $i = 2 - x, y, 1/2 - z$)

Fe1	O7	2.015(2)	
Fe1	O7^i	2.015(2)	
Fe1	O1	2.053(2)	
Fe1	O1^i	2.053(2)	
Fe1	N6	2.101(4)	
Fe1	O2	2.172(3)	
Fe1	O2^i	2.172(3)	
O7	Fe1	O7^i	177.64(12)
O7	Fe1	O1	90.89(9)
O7^i	Fe1	O1	89.74(9)
O7	Fe1	O1^i	89.73(9)
O7^i	Fe1	O1^i	90.89(9)
O1	Fe1	O1^i	149.29(13)
O7	Fe1	N6	91.18(6)
O7^i	Fe1	N6	91.18(6)
O1	Fe1	N6	74.64(7)
O1^i	Fe1	N6	74.64(7)
O7	Fe1	O2	88.78(10)
O7^i	Fe1	O2	89.17(10)
O1	Fe1	O2	76.03(11)
O1^i	Fe1	O2	134.68(11)
N6	Fe1	O2	150.67(9)
O7	Fe1	O2^i	89.17(10)

2poapz chelating to the seven-coordinate pentagonal bipyramidal metal in a tridentate NO_2 fashion. A bidentate nitrate provides two oxygen donor atoms in the pentagonal plane, and two water molecules occupy axial positions. In plane contacts are short (<2.06 Å), with longer axial contacts (2.172(3) Å), suggesting HS Fe(III) (*vide supra*). The end pockets of the ligand are uncoordinated, and the ligand adopts a planar conformation, stabilized by hydrogen bonding interactions (dotted lines, Figure 2) involving the N−H protons and the hydrazone oxygen and pyrazine 2-nitrogen atoms (N−H 2.254 Å, O−H 2.243 Å).

*$[(2poapz\text{-}H)_4Fe_4](NO_3)_6\cdot 9H_2O$ (**2**).* The molecular structure of **2** is shown in Figure 3a. Crystallographic details are given in Table 1 and important distances and angles in Table 3. In contrast to the structure of **1**, complex **2** has a tetranuclear grid based structure with four Fe centers bridged by four hydrazone oxygen atoms, assembled from four ligands which bind via one end only in a pin-wheel fashion. The structure resembles that obtained in many cases with simple ditopic hydrazone ligands based on 2-picolinic hydrazone.[1−3] The central

Table 3. Selected Distances (Å) and Angles (deg) for 2

Fe1	N26	2.049(5)	
Fe1	N4	2.077(5)	
Fe1	O1	2.118(4)	
Fe1	O5	2.143(4)	
Fe1	N1	2.174(6)	
Fe1	N23	2.203(5)	
Fe2	O2	1.972(5)	
Fe2	O1	2.009(4)	
Fe2	O7	2.018(4)	
Fe2	O8	2.037(4)	
Fe2	N39	2.074(5)	
Fe2	N6	2.085(5)	
Fe3	N15	2.036(5)	
Fe3	N37	2.060(5)	
Fe3	O3	2.138(4)	
Fe3	N34	2.171(5)	
Fe3	O7	2.214(4)	
Fe3	N12	2.259(6)	
Fe4	O4	1.991(5)	
Fe4	O6	1.992(4)	
Fe4	O3	2.041(4)	
Fe4	O5	2.050(4)	
Fe4	N17	2.062(5)	
Fe4	N28	2.068(4)	
Fe2	O1	Fe1	128.42(19)
Fe4	O3	Fe3	130.55(18)
Fe4	O5	Fe1	130.34(18)
Fe2	O7	Fe3	128.37(19)

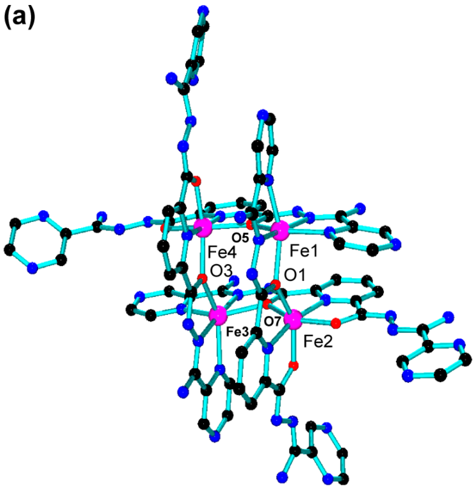

Figure 3. (a) Structural representation of the Fe_4 grid cation in $[(2poapz\text{-}H)_4Fe_4](NO_3)_6\cdot 9H_2O$ (**2**). (b) Structural representation of the $Fe_4(\mu\text{-}O)_4$ core in $[(2poapz\text{-}H)_4Fe_4](NO_3)_6\cdot 9H_2O$ (**2**).

pyridine subunit provides both bridging and terminal metal-hydrazone oxygen bonds to the Fe centers. The core structure showing the μ_2-O bridging is shown in Figure 3b. Two Fe centers (Fe1, Fe3) have N_4O_2 coordination spheres, and the other two (Fe2, Fe4) have N_2O_4 coordination spheres. BVS calculations[36] show dramatic differences depending on the coordination sphere composition (Fe2 3.01, Fe4 3.01, Fe1 2.24, Fe3 2.14) indicating two HS Fe(III) centers (Fe2, Fe4) and two HS Fe(II) centers (Fe1, Fe3) (*vide infra*). This would nominally agree with the coordination site composition based on the N and O content but is somewhat of a surprise given the fact that the metal starting material was Fe(III)(NO_3)$_3$. The reducing conditions could have resulted from the presence of acetontrile in the solvent and the resulting stabilizing influence provided by the N_4O_2 coordination environment at the Fe(II) sites. The fact that only one end of each ligand coordinates may be associated with the weaker donor properties associated with the terminal pyrazine rings (see the following discussion on complexes of related ligands with terminal pyridine rings). This is corroborated by the formation of complex **1** also in the reaction of 2poapz with Fe(III)(NO_3)$_3$.

[(2poap)$_6$Fe$_9$](ClO$_4$)$_8$·18H$_2$O (**3**). The molecular structure of **3** is shown in Figure 4. Crystallographic details are given in Table 1 and important distances and angles in Table 4. The structure reveals a complete [3 × 3] Fe$_9$ square grid, with the expected arrangement of nine metal ions and six 2poap ligands in two roughly parallel groupings of three on either side of the grid faces. The Fe analysis is also consistent with the presence of nine Fe atoms (*vide supra*). Each ligand acts in a tritopic, heptadentate fashion with the hydrazone oxygen atoms bridging adjacent Fe centers. Figure 5 shows the core structure involving just the immediate donor atoms. Although Figure 5 appears to portray a fairly flat grid, it is in reality quite puckered, as shown in the side on view in Figure 6. The stucture reveals eight ClO$_4^-$ ions, which is consistent with the elemental analysis, and suggests that some Fe oxidation has occurred (comparable Mn(II)$_9$ [3 × 3] grids consistently show six monoanions indicating a preferred loss of two protons per ligand). Examination of the Fe−L distances reveals that for Fe3, Fe4, and Fe9 shorter bonds exist on average than for the other sites. BVS calculations[36] for these metal ions (2.71, 2.70, 2.76, respectively) are high, suggesting HS Fe(III), while lower values for the other sites are consistent with HS Fe(II). In this context, it is important to note that the space group ($P\bar{1}$) indicates that there is no effective symmetry within the [3 × 3] grid itself. This is in contrast to the situation for the putative [3 × 3] grid system with the ligand Cl2poap (*vide infra*). While the loss of two protons per ligand is normal (*vide supra*), additional proton loss can occur when Fe(III) is present. In the present case, if three Fe(III) sites exist, one extra proton will be lost from the group of six ligands. Pinpointing the site of extra proton loss from structural data is not possible and also cannot be confirmed from the elemental analysis. However, proton loss would most reasonably occur at an amidrazone NH$_2$ group, and the resulting anionic site would be stabilized through canonical contributions resulting from double bond delocalization along the ligand backbone. Fe−O−Fe bridge angles fall in the range 130.6−134.7°, consistent with antiferromagnetic exchange within the grid (*vide infra*).

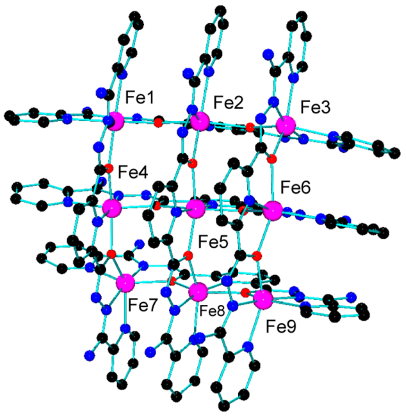

Figure 4. Structural representation of the Fe$_9$ grid cation in [(2poap)$_6$Fe$_9$](ClO$_4$)$_8$·18H$_2$O (**3**).

Putative [3 × 3] Grids with the Ligand Cl2poap. Several reactions of Cl2poap with Fe(II)(ClO$_4$)$_2$ were carried out under varying conditions, chosen to try to produce an unoxidized Fe(II)$_9$ grid by using oxygen free reaction conditions and adding reducing agents. Grid based Fe$_9$ structures (**4a**−**4c**) and one incomplete, but grid-like, Fe$_6$ structure (**5**) were obtained. **4a**−**c** were obtained as major products with the same space group ($P4_2/n$ (#86)), essentially the same cell dimensions, and similar magnetic properties (*vide infra*), and so are generally equivalent. The Fe$_6$ incomplete grid structure (**5**) was observed as a soluble crystalline product from the mother liquor in the reaction of Cl2poap with Fe(ClO$_4$)$_2$. This suggests a possible Fe$_6$ intermediate in the full grid assembly. Since the structures of **4a**−**4c** are essentially the same, only one (**4a**) is discussed in detail and is considered to be representative of the group. The initial structural refinements on **4a**−**4c** gave large R_1 values (∼13%), and the thermal ellipsoids for the four equivalent side Fe centers, based on unit occupancy, were found to be large and distorted, suggesting a problem with the structures. Other information, for example Fe analysis (*vide supra*) and variable temperature magnetic data (*vide infra*), suggested that the occupancy of the side grid sites might not be unit, and in fact substantially less. Consequently, new refinements were carried out which allowed the occupancy levels of the side sites to vary. This lead to less than unit occupancy at the symmetry equivalent side grid sites, greatly improved refinement values, and normal thermal ellipsoids at these sites (*vide infra*). The nominal Fe2 site occupancies obtained through this variable occupancy refinement are 0.46, 0.62, and 0.60 respectively for **4a**−**4c** (for R1 values of 0.0972, 0.0763, and 0.0814, respectively). In the case of **4a**, the structure was refined anisotropically, without using a solvent mask, revealing eight perchlorates per grid in the lattice. However, for **4b** and **4c**, a solvent mask was employed, and although the eight expected perchlorates could not be unambiguously found from examination of difference maps, they could be accommodated in the void volume and are reasonably assigned to the electrons therein. Crystallographic data for **4a** are included in Table 1, and details for **4b** and **4c** are included in Table S1.

[(Cl2poap)$_6$Fe$_7$](ClO$_4$)$_8$·15H$_2$O (**4a**). The structure of the cation in **4a** is shown in Figure 7, and the core framework involving just the immediate donor atoms in shown in Figure 8. Crystallographic parameters are given in Table 1, and important bond distances and angles are listed in Table 5. The grid has 4-fold symmetry (space group $P4_2/n$), indicating that the corner sites are all equivalent and the side sites are also equivalent. Six ligands and nine metal sites are arranged in the typical [3 × 3] grid fashion with all metals linked through 12 μ-O$_{\text{hydrazone}}$ bridges. The symmetry equivalent corner sites and the center site represent Fe atoms with unit occupancy. However, despite the equivalence of the side sites, the Fe atoms are only present at approximately half the expected unit occupancy based on the refinement statistics (*vide infra*). The symmetry indicates that all the sites are equivalent on the time scale of the X-ray diffraction experiment. The overall grid dimensions are close to those observed for other typical [3 × 3] grids with other transition metal ions. Fe−L bond distances at the center (Fe3) and corner (Fe1) sites are short (2.026(4) Å$_{\text{ave}}$, 2.059(5) Å$_{\text{ave}}$ respectively), and BVS values[36] (Table 6; 3.11, 3.16 respectively) are consistent with HS Fe(III). Fe−L distances at the Fe2 side sites vary widely in the range 1.95−2.41 Å (2.148(5) Å$_{\text{ave}}$), with the long contacts to the terminal pyridine rings. The BVS value[36] (2.94) might suggest HS Fe(III) at these sites, but this is inconsistent with other data (*vide infra*), which suggest HS Fe(II). The incomplete site occupancy would no doubt contribute to this unusual situation. Fe−O−Fe bridge angles fall in the range 133−136°.

Our experience with [3 × 3] grids with related ligands and other metal ions (e.g., Mn(II), Cu(II)) shows that despite normal types of mixed NO donor groupings within the grids, metal−ligand distances are typically not what would be anticipated based on simpler mononuclear species or even dinuclear complexes with related smaller chelating ligands. We attribute this to the repulsion effects generated as

Table 4. Selected distances (Å) and Angles (deg) for 3

Fe1	N30	2.053(7)	Fe6	O12		2.194(5)
Fe1	N3	2.067(7)	Fe6	N18		2.236(6)
Fe1	O1	2.110(6)	Fe6	O11		2.254(5)
Fe1	O7	2.205(5)	Fe7	N21		2.052(6)
Fe1	N1	2.210(7)	Fe7	N34		2.085(6)
Fe1	N28	2.222(7)	Fe7	O5		2.165(5)
Fe2	N39	2.047(7)	Fe7	O8		2.188(5)
Fe2	N5	2.071(7)	Fe7	N19		2.210(6)
Fe2	O1	2.130(5)	Fe7	N36		2.257(6)
Fe2	O9	2.148(5)	Fe8	N43		2.047(6)
Fe2	N37	2.265(8)	Fe8	N23		2.092(6)
Fe2	O2	2.280(5)	Fe8	O5		2.093(5)
Fe3	N48	2.024(7)	Fe8	O10		2.094(5)
Fe3	O11	2.051(5)	Fe8	N45		2.215(6)
Fe3	N7	2.061(7)	Fe8	O6		2.297(5)
Fe3	O2	2.064(5)	Fe9	N25		2.015(6)
Fe3	N9	2.180(6)	Fe9	N52		2.040(6)
Fe3	N46	2.191(7)	Fe9	O12		2.045(5)
Fe4	N12	2.027(6)	Fe9	O6		2.054(5)
Fe4	O3	2.048(5)	Fe9	N54		2.168(6)
Fe4	N32	2.067(6)	Fe9	N27		2.215(6)
Fe4	O7	2.089(5)	Fe1	O1	Fe2	130.6(3)
Fe4	O8	2.090(5)	Fe3	O2	Fe2	133.0(3)
Fe4	N10	2.207(6)	Fe4	O3	Fe5	133.9(2)
Fe5	N41	2.050(6)	Fe6	O4	Fe5	133.1(2)
Fe5	N14	2.091(6)	Fe8	O5	Fe7	131.0(2)
Fe5	O9	2.109(5)	Fe9	O6	Fe8	133.5(2)
Fe5	O4	2.137(5)	Fe4	O7	Fe1	133.3(2)
Fe5	O10	2.142(5)	Fe4	O8	Fe7	131.2(2)
Fe5	O3	2.229(5)	Fe5	O9	Fe2	134.7(3)
Fe6	N16	2.049(6)	Fe8	O10	Fe5	130.8(2)
Fe6	N50	2.095(6)	Fe3	O11	Fe6	132.7(3)
Fe6	O4	2.112(5)	Fe9	O12	Fe6	132.5(2)

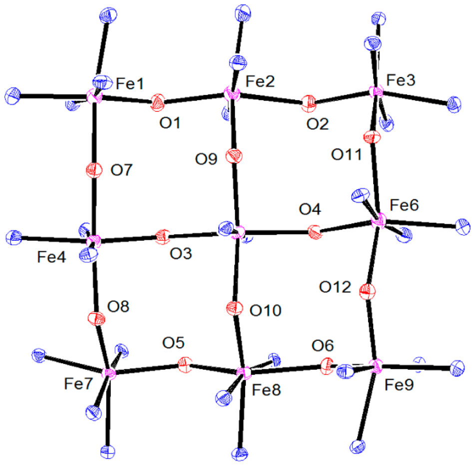

Figure 5. Structural representation of the $Fe_9(\mu\text{-}O)_{12}$ core in $[(2poap)_6Fe_9](ClO_4)_8 \cdot 18H_2O$ (3).

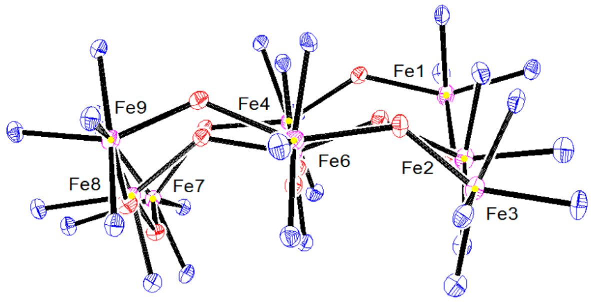

Figure 6. Structural representation of the $Fe_9(\mu\text{-}O)_{12}$ core in (3) (side view).

the six ligands approach each other in their respective grid positions, which tends to make M−L bonds longer than anticipated, particularly at the side sites. It is useful to compare the structure of **4a** (and **4b**, **4c**) with the related pentanuclear complex $[(Cl2poap)_6Fe(III)_5](ClO_4)_9$, which was obtained by reaction of Cl2poap with $Fe(ClO_4)_3$. It has an unusual pentanuclear incomplete grid structure with Fe(III) ions occupying just the corner and center sites, and metal free "vacant" N_3O_3 coordination sites at the side positions, but a "normal" [3 × 3] arrangement of the six ligands. Bond lengths and magnetic and Mössbauer properties in this case are consistent with all HS Fe(III) sites (BVS values in the range 3.0−3.15).[11] This distribution of Fe(III) sites mirrors that in **4a**−**4c**. It is of interest to note that it has not been possible to produce a [3 × 3] Fe grid with all Fe(III) sites under any reaction conditions, which may be due to possible ligand based steric congestion which would inevitably result from the shorter bond lengths at all the Fe(III) sites in a putative $Fe(III)_9$ grid.

Additional information to support the unusual spin state distribution can be obtained from the elemental analysis. The results are consistent with a nominal net charge on the metal grid cation of +8, in agreement with the number of perchlorate anions observed directly in the structure of **4a**. Normally, ligands of this type lose two hydrazone protons easily, commonly leading to a −2 ligand charge in the complex. However, in the case of $[(Cl2poap)_6Fe(III)_5]$ $(ClO_4)_9$,[11] a sensible charge balance requires that each ligand loses only one

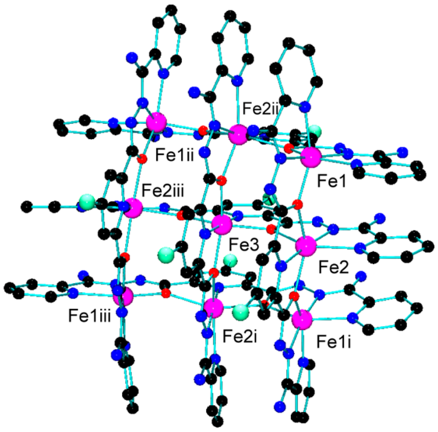

Figure 7. Structural representation of the grid cation in [(Cl2poap)$_6$Fe$_7$](ClO$_4$)$_8$·15H$_2$O (**4a**).

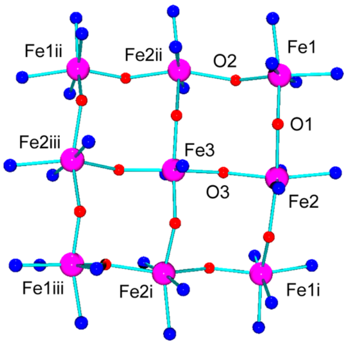

Figure 8. Structural representation of the grid core in [(Cl2poap)$_6$Fe$_7$](ClO$_4$)$_8$·15H$_2$O (**4a**).

Table 5. Selected Distances (Å) and Angles (deg) for 4a

Fe1	O1	2.002(4)	Fe2	N12	1.887(5)	
Fe1	O2	2.002(4)	Fe3	O3	2.013(3)	
Fe1	N1	2.157(5)	Fe3	O3	2.013(3)	
Fe1	N3	2.030(5)	Fe3	O3	2.013(4)	
Fe1	N7	2.022(5)	Fe3	O3	2.013(3)	
Fe1	N9	2.154(5)	Fe3	N14	2.051(6)	
Fe2	O1	2.241(4)	Fe3	N14	2.051(6)	
Fe2	O2	2.222(4)	Fe1	O1	Fe2	133.32(19)
Fe2	O3	2.171(4)	Fe1	O2	Fe2	135.81(19)
Fe2	N5	1.956(5)	Fe3	O3	Fe2	135.94(19)
Fe2	N10	2.408(9)				

Table 6. BVS Calculations for 4a−4c

	Fe1 (corner)	Fe2 (side)	Fe3 (center)
(**4a**) (120 K)	3.16	2.94	3.11
(**4b**) (193 K)	3.15	2.35	2.69
(**4c**) (193 K)	3.06	2.38	2.63

proton. The NH$_2$ groups can also dissociate, leading to additional ligand negative charge. Considering **4a**, in the absence of such additional dissociation, the nominal metal based cation charge would be +20, assuming the presence of eight perchlorate anions. Given the presence of five HS Fe(III) sites (*vide supra*), the only way in which the side sites are present as Fe(II) is if these sites are incompletely occupied. The occupancy from the structure suggests ~50% Fe(II) at the side sites leading to a net metal based charge of +19 (Fe(III)$_5$Fe(II)$_2$). On the assumption that the structure is representative of the bulk sample, the charge discrepancy can be explained by slightly less ligand proton dissociation. In the case of **4b** and **4c**, slightly more ligand proton dissociation would be required. The elemental analysis for **4c** includes both Fe and Cl (*vide supra*), adding strong support to the occupancy at Fe(2) of ~0.6.

The presence of mixed oxidation state grid sites has been observed before with oxidized Mn(II)$_9$ [3 × 3] grids with this type of ligand, where oxidation occurs readily at the equivalent corner sites giving both fully (4e) oxidized grids but also partially oxidized grids, where varying numbers of these equivalent sites can be oxidized (*vide supra*). However, the accumulated charge is evenly spread over the four corner sites, as indicated by crystal symmetry, 4-fold grid symmetry, and magnetic properties.[3d,13]

***[(Cl2poap)$_6$Fe$_{7.5}$](ClO$_4$)$_8$·14H$_2$O* (4b), *[(Cl2poap)$_6$Fe$_{7.4}$](ClO$_4$)$_8$·22H$_2$O* (4c).** Crystallographic data for **4b** and **4c** are listed in Table S1, and bond distances and angles are listed in Tables S2 and S3. The structures of the cations in **4b** and **4c** are essentially identical to that in **4a**. Structural representations are given in Figures S1 and S2, respectively. **4b** and **4c** both crystallize in the tetragonal system (space group $P4_2/n$), and so as with **4a** the grids have effective 4-fold symmetry, indicating that the corner sites are all equivalent and the side sites are also equivalent. BVS values based on the new refinements (Table 6) are consistent with five HS Fe(III) sites at the corners and center, but the values for the side sites are smaller than for **4a** but consistent with the presence of HS Fe(II). However, it is not clear to what extent the refined site dimensions based on occupancies of <1 would affect the BVS values. Further evidence for HS Fe(II) at the Fe2 side sites in **4c** comes from the Mössbauer data (*vide infra*).

***[(Cl2poap)$_5$Fe$_6$](ClO$_4$)$_8$·20H$_2$O* (5).** The molecular structure of **5** is shown in Figure 9. Crystallographic details are given in Table 1 and important distances and angles in Table 7. The cluster assembly is an unusual rectangular hexanuclear structure involving five ligands and six metal ions. The Fe atoms are arranged in two linear trinuclear groupings at the ends of the rectangle, with one ligand acting in the expected tritopic fashion binding three metals in each case. Three additional ligands link the well separated trinuclear subunits, acting in a remote ditopic fashion, with the central pockets vacant in all cases. These ligands are almost parallel and the uncomplexed pyridine rings almost eclipsed with a slight offset. What is significant is that the ligand *cisoid* conformations mirror what would occur in a fully metalated [3 × 3] grid, but the central triad of metals is missing. This is germane to the possible grid assembly mechanism (*vide infra*). Inter-ring contacts are quite short in the range 3.4−3.7 Å, suggesting significant π type interactions. Fe-ligand contacts fall into two groups with a distinction between Fe sites based on BVS calculations[36] (Fe1 2.57, Fe2 3.08, Fe3 2.53, Fe4 3.14, Fe5 2.36, Fe6 3.18). Fe2, Fe4, and Fe6 are clearly Fe(III), while the other values suggest that the Fe sites are not Fe(III), and despite the higher than expected values are assigned to Fe(II),

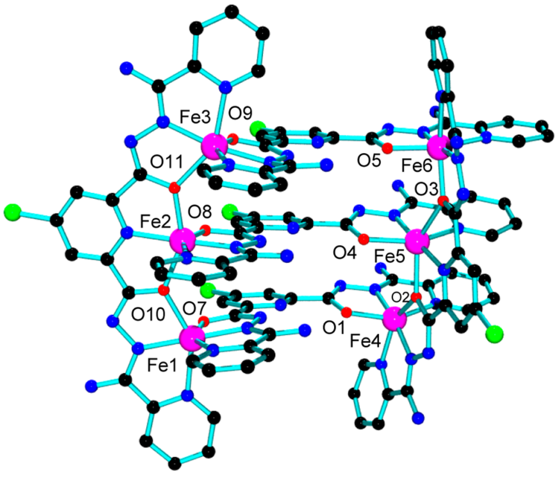

Figure 9. Structural representation of the incomplete grid in [(Cl2poap)$_5$Fe$_6$](ClO$_4$)$_8$·20H$_2$O (**5**).

Table 7. Selected Distances (Å) and Angles (deg) for 5

Fe(1)−N(41)	2.051(3)
Fe(1)−N(27)	2.093(3)
Fe(1)−O(7)	2.156(2)
Fe(1)−N(29)	2.162(3)
Fe(1)−O(10)	2.194(2)
Fe(1)−N(40)	2.203(3)
Fe(2)−O(8)	1.973(2)
Fe(2)−N(31)	2.005(3)
Fe(2)−O(10)	2.036(2)
Fe(2)−O(11)	2.048(2)
Fe(2)−N(43)	2.070(3)
Fe(2)−N(33)	2.176(3)
Fe(3)−N(45)	2.053(3)
Fe(3)−N(35)	2.093(3)
Fe(3)−O(11)	2.154(2)
Fe(3)−O(9)	2.159(2)
Fe(3)−N(37)	2.202(3)
Fe(3)−N(46)	2.224(3)
Fe(4)−O(1)	1.978(2)
Fe(4)−N(5)	2.010(3)
Fe(4)−N(11)	2.021(3)
Fe(4)−O(2)	2.025(3)
Fe(4)−N(7)	2.144(3)
Fe(4)−N(10)	2.209(3)
Fe(5)−N(19)	2.048(3)
Fe(5)−O(4)	2.098(2)
Fe(5)−N(13)	2.119(3)
Fe(5)−N(17)	2.202(3)
Fe(5)−O(2)	2.234(2)
Fe(5)−O(3)	2.283(2)
Fe(6)−O(5)	1.975(2)
Fe(6)−N(15)	2.018(3)
Fe(6)−N(23)	2.026(3)
Fe(6)−O(3)	2.033(2)
Fe(6)−N(21)	2.131(3)
Fe(4)−O(2)−Fe(5)	130.74(12)
Fe(6)−O(3)−Fe(5)	131.00(11)
Fe(2)−O(10)−Fe(1)	131.27(10)
Fe(2)−O(11)−Fe(3)	129.38(11)

based on a reasonable charge balance assessment and magnetic data (*vide infra*). Elemental analysis and the structure indicate the presence of eight perchlorates, and on the basis of the two terminal ligands having −2 charge, as expected, and the others having −1 each, a charge balance is achieved.

Within each trinuclear subunit, the Fe centers are separated by distances in the range 3.79−3.93 Å and are bridged by hydrazone oxygen atoms with Fe−O−Fe bridge angles in the range 129−132°. These connections would suggest intramolecular antiferromagnetic exchange (*vide infra*). It is not immediately obvious why this unusual incomplete grid structure exists, but it points to the fact that there are several different ways in which the metal ions and ligands interact. This will depend on reaction conditions, the identity of the ligand, and differing assembly pathways and directional effects associated with the different metal ion sizes (e.g., Fe(II) vs Fe(III)) and the coordination pocket composition. Also, the effective grid-like array of ligands and the missing central group of metals suggest such a species as a possible intermediate in the full grid assembly (*vide infra*).

Grid Assembly Mechanism. Mn(II) vs Fe(II) vs Fe(III) vs the Ligand. Mn(II) chemistry with Cl2poap and other closely related picolinic-2,6-bis-hydrazone ligands is well documented, and the Mn_9 complexes can be produced in high yield.[10−13] The Mn(II) sites have unit occupancy, indicating that in the grid assembly process there is a roughly equal chance of the +2 charged metal ions occupying any of the grid positions. Also, since Mn(II) has no Crystal Field Stabilization Energy (CFSE), there would be no preference for a particular coordination environment (N_4O_2 (corner), N_3O_3 (side), or N_2O_4 (center)). Quantifying the assembly process is, of course, difficult, but with Mn(II) no examples of incompletely metalated grid intermediates have so far been isolated, which could possibly indicate a particular assembly mechanism.

In the case of Fe(II), one could perhaps assume a similar grid assembly mechanism, but the susceptibility of Fe(II) to oxidation to Fe(III) would clearly influence the process and also there would likely be a small CFSE preference, which might direct Fe(II) to more nitrogen rich sites. Given the apparent incomplete incorporation of Fe(II) at the side sites, and unit occupancy of the corner and center Fe(III) sites in **4a**−**4c**, it suggests that the center and corner sites are the first to be occupied. If the corner and center sites undergo oxidation to Fe(III) either before or during assembly, this would have the effect of drawing the ligands in more closely due to the shorter Fe−L distances, and this would tend to inhibit incorporation of metal ions at the side sites. The mechanism of Fe(II) oxidation is not clear but probably results from incomplete exclusion of air during synthesis and work up, despite efforts to prevent this happening. However, the unusual reduction of Fe(III) in the case of **2** indicates that redox processes may also be influenced significantly by the coordination environment at a particular grid site and possible sacrificial endogenous redox agents.

In the context of a possible mechanism, complex **5** may provide some clues, since this intermediate was isolated from the mother liquor after the initial precipitation of what appeared to be the "full" grid and was clearly more soluble. The two trinuclear end groups coordinated to a ligand framework composed of three parallel ligands and two end cross ligands resembles a partial grid with a ligand and three metals missing. The fact that the middle metal triad is not present suggests that the corner sites are occupied first. This would be consistent with the probable desire of Fe(II) to occupy more nitrogen rich sites initially, given its softer Lewis acid character compared with Fe(III). The fact that three of the corner sites are oxidized may be a reflection on the more exposed nature of these sites in the presence of trace amounts of oxygen. The missing metal ions in the middle row may be a reflection on the donor character of the central pyridine ring. The 4-chloro substituent would have a significant electron withdrawing influence on the donor character of the nitrogen atom and thus make it a weaker donor. In the final step of a putative assembly mechanism, the last ligand and the remaining three metals would be added. The oxidation of the central Fe(II) may occur separately in a simple mononuclear intermediate, which would fit into the available central portion. If this intermediate had a structure similar to **1**, the ligand would be in the correct conformation to provide the appropriate coordination environments for the incorporation of the final two metal ions. Addition of these Fe(II) ions would likely occur sequentially but of necessity would be hindered by the presence of the last ligand. The fact that a full grid was obtained in the case of **3**, with no detectable intermediates, involving the closely related parent ligand with no 4-Cl substituent, adds weight to this argument, since the central pyridine nitrogen atoms would be stronger donors.

Mössbauer Spectroscopy. ***Evidence for HS Fe(III) and HS Fe(II).*** The Mössbauer spectra[37] for **4c** at variable temperature (Figure 10, Table S4) show evidence for the presence of both HS Fe(III) and HS Fe(II) sites. The spectra were initially analyzed assuming the superposition of three doublets assigned to the unique grid groupings of HS Fe(III) sites (one Fe(3) (center), four Fe(1) (corners)) and four putative Fe(II) sites (Fe(2) (side)), assuming 4-fold grid symmetry and unit occupancy at each metal site (*vide supra*). If the nine crystallographic sites have the same recoil-free fraction at all temperatures, one would expect three doublets with an area ratio of 1:4:4 for Fe(3), Fe(1), and Fe(2), respectively, for the equivalent groupings of metal centers. The spectral analysis at all temperatures from 250 to 25 K failed to fit this ratio. Given the results of the structural analysis, where the Fe(III) sites are at unit occupancy, and the Fe(II) sites are present at less than unit occupancy, this is perhaps not surprising. The hyperfine parameters (Table S4) suggest that if

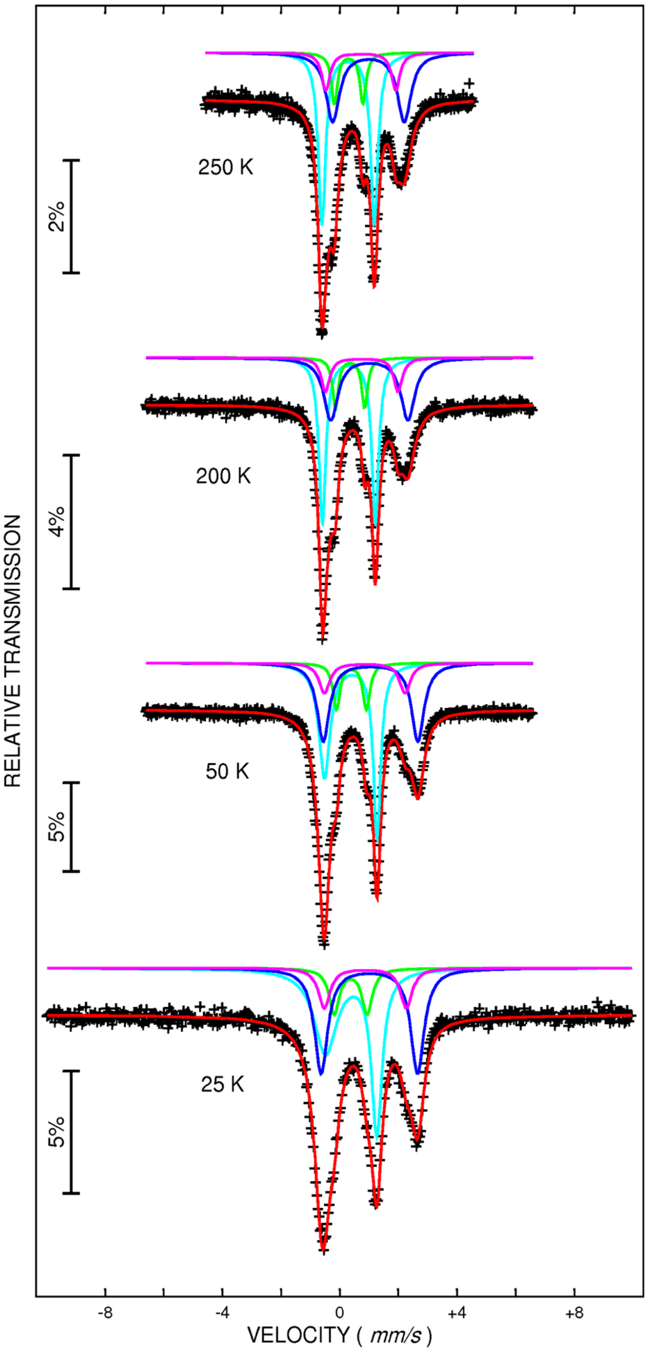

Figure 10. The ^{57}Fe Mössbauer spectra of **4c** at indicated temperatures.

there are five high-spin (HS) Fe(III) sites, the absorptions associated with the Fe(II) centers appear to be present in two groups, with three sites (dark blue trace, Figure 10) and one other (pink trace, Figure 10) in a nominal ratio of 3:1. The very broad absorption at ∼+2.5 mm/s and a clear shoulder at ∼+2.0 mm/s indicate that in this compound there are different types of Fe(II) HS species. The structure indicates that the Fe(II) centers are crystallographically identical, which is presumably due to the different times scales of the two techniques, and the averaged structural situation. In addition, the two different iron(II) sites observed by Mössbauer spectroscopy are present at both high and low temperatures. Such behavior is not unusual and has been observed before.[38] There is no marked deviation of the values of the hyperfine parameters from 250 K to low temperatures.

The hyperfine parameters show that the isomer shifts for the doublets assigned to Fe(III) are reasonable for high-spin Fe(III) ions and are rather similar. An increase in the isomer shift upon cooling is attributed to the second-order Doppler effect. The quadrupole splittings (ΔE_Q) show little dependence upon temperature between 250 and 25 K, as expected for high-spin Fe(III) ions for which the quadrupole interaction arises only from a lattice contribution to the electric field gradient at the iron center. A different situation exists for the Fe(II) quadrupole splitting values, which are temperature dependent. Such changes in ΔE_Q with temperature are not unexpected, and they are the result of rearrangement in the thermal population of the large number of spin−orbit states involved. At low temperatures, the fit was only possible with one of the doublets assigned to Fe(III) being asymmetric, although the fit with the asymmetry assigned to peripheral Fe(II) ions gave similar values. At first sight, it can suggest a change in sign of the V_{zz} component of the EFG tensors, but a physical reason for such temperature dependence is problematic. Moreover, it is not completely clear for which iron sites this change is more probable. An explanation might be hidden in the presence of two slightly different Fe(II) ions, and the appearance of such asymmetry may indicate that there could also be some lattice transformations which influence the asymmetry of the peaks. An alternative explanation for the line asymmetry could be due to low temperature intermediate relaxation for the Fe(III) ions, which is supported by the line broadening of the doublets assigned to these ions with decreasing temperature.

However, in this context, the presence of two resolved doublets associated with Fe(II), with one nominally assigned to three sites, can be interpreted in terms of a predominance of grids with five HS Fe(III) sites and three side sites occupied by HS Fe(II). This would be consistent with the structural data (*vide supra*). Given that other grid species with different side site occupancies would also exist on statistical grounds, the weaker doublet could be due to the presence of grids with less average Fe(II) content, in which slightly different Fe(II)N_3O_3 coordination geometries exist. Specifically identifying the substituted grids is somewhat problematic given the averaged situations which would exist based on the structural and magnetic properties (*vide infra*). With this in mind, the 50 K Mössbauer data were re-examined, with the Fe(III) sites assumed to be at unit occupancy and allowing the Fe(II) occupancy to vary. A nominal ratio of Fe(III)/Fe(II) of 60/40 was obtained, indicating that there is a larger relative proportion of Fe(III) sites compared to Fe(II) (calculated Fe(III)/Fe(II) ratio assuming unit occupancy at each site is 55.6%). The obvious discrepancy between this analysis and the rerefined structural data is not immediately obvious, but given the relatively high R1 values (>0.076), some measure of flexibility in the site occupancies might be expected. The question of the structures being based on single crystal data and the magnetic and Mössbauer data on bulk samples should be considered and could lead to differences in the assessed site occupancies. However, the general consistency between the structural and bulk magnetic data suggests otherwise.

Variable temperature Mössbauer spectra were also obtained for **4b**, displaying similar features to **4c**, indicative of a similar mixture of HS Fe(III) and HS Fe(II) sites. The spectra at 77 and 293 K are shown in Figures S3 and S4, respectively, for comparison with **4c**. Slight differences in relative intensities of some absorption features were observed, which is not unexpected given the slight differences in structural and magnetic properties of **4b** and **4c**. The major feature at ∼0 mm/s at 293 K is resolved into two peaks, which may reflect the temperature dependence of ΔE_Q for Fe(II) (*vide supra*).

Magnetic Properties. Variable temperature magnetic data for **1** are shown in Figure S5 and reveal a roughly constant magnetic moment (6.1 μ_B) from 300 K down to ∼30 K, followed by a slight drop to 4.8 μ_B at 2 K, typical of a mononuclear HS Fe(III) system.

Variable temperature magnetic data for **2** are shown in Figure 11 as a plot of μ_{mol} as a function of temperature. The moment drops from 9.4 μ_B at 300 K to a plateau value of 5.7 μ_B from ∼30 to 10 K, followed by a slight additional drop to 5.3 μ_B at 2 K. The overall drop in moment signals the presence of intramolecular antiferromagnetic exchange, but the plateau at 5.7 μ_B is not consistent with an exchange model based on a symmetric disposition of two HS Fe(II) and two HS

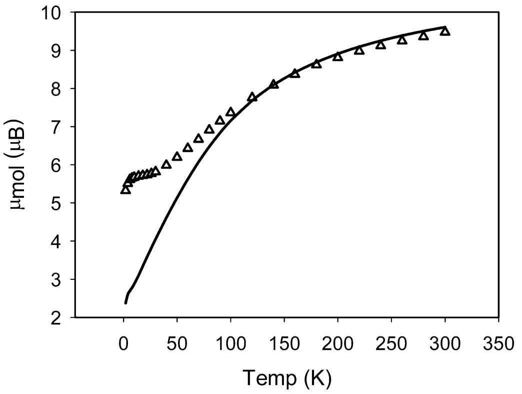

Figure 11. Variable temperature magnetic data for $[(2poapz\text{-}H)_4Fe_4](NO_3)_6{\cdot}9H_2O$ (**2**) (see text for fitted parameters).

Fe(III) centers (eq 1; $S_1 = S_3 = 5/2$, $S_2 = S_4 = 4/2$). For such a model, the ground state spin would be $S = 2/2$, in disagreement with the magnetic data. However, a trial fit of the data to eq 1

$$H_{ex} = -J\{S_1{\cdot}S_2 + S_2{\cdot}S_3 + S_3{\cdot}S_4 + S_1{\cdot}S_4\} \quad (1)$$

was attempted using MAGMUN4.1[39] and found to fit quite well above 100 K (solid line in Figure 11 for $g_{ave} = 2.05$, $J = -13$ cm^{-1}, TIP = 200 × 10^{-6} cm^3 mol^{-1}, $\theta = -1$ K; TIP = temperature independent paramagnetism, θ = Weiss correction). Divergence from this model occurred at ~100 K (NB the X-ray structure was determined at 163 K). Use of just one J value is reasonable given the structure and the similar Fe−O−Fe bridge angles. In order for the low temperature moment to be higher than the calculated values using this model, a higher nominal ground state spin is required. Assuming a ferrimagnetic situation prevails, the only way to have such an increase in ground state spin is for a spin crossover change to occur at one or more sites. On the assumption that the most likely candidates would be the HS Fe(II) sites, attempts were made to model the low temperature regime (<100 K) using models where one and two HS Fe(II) sites became low spin (LS). The only model which fit the data is one where there is a fairly abrupt HS ← →LS crossover of just one Fe(II) site (eq 1, e.g. $S_4 = 0$), corresponding to exchange Hamiltonian 2 ($S_1 = S_3 = 5/2$; $S_2 = 4/2$).

$$H_{ex} = -J1\{S_1{\cdot}S_2 + S_2{\cdot}S_3\} - J2\{S_1{\cdot}S_3\} \quad (2)$$

However, a good fit was only possible with the inclusion of a small secondary exchange term between the two $S = 5/2$ centers. The fit gave $g_{ave} = 2.03(1)$, $J1 = -13(1)$ cm^{-1}, $J2 = -5.2(1)$ cm^{-1}, $\theta = -0.8$ K, $10^2R = 1.7$. The experimental data and fitted line are shown in Figure 12a, as plots of μ_{mol} as a function of temperature. Re-evaluation of the region >100 K using eq 1 is shown in Figure 12b, as plots of μ_{mol} as a function of temperature ($g_{ave} = 2.01(1)$, $J = -12.0(1)$ cm^{-1}, $\theta = 0$ K, $10^2R = 1.5$). The solid line is calculated with the fitted parameters.

Variable temperature magnetic data for **3** are shown in Figure 13 as a plot of μ_{mol} as a function of temperature. The value at 300 K is 14.4 μ_B dropping steadily to a slight shoulder value of ~7.1 μ_B at ~10 K, followed by a drop to 5.5 μ_B at 2 K. The overall drop signifies intragrid antiferromagnetic exchange, with the nonzero value at 2 K implying residual ground state spin. On the assumption that there are three HS Fe(III) sites (Fe3, Fe4, Fe9; *vide supra*), it is possible to predict the ground state spin. Figure 14 shows a number of spin models for hypothetical [3 × 3] grids with mixtures of HS Fe(II) and HS Fe(III) centers. The present example can be represented by case 6 (integer spin numbers). Assuming antiferromagnetic exchange throughout the grid, and taking into account coupling between adjacent spin centers only, the sum of the residual spins in the ground state is 4/2 + 3 × 1/2 = 7/2. The calculated spin-only value for this situation (7.9 μ_B) is slightly higher than the shoulder value (7.1 μ_B), supporting the spin distribution. The room temperature spin only value for this spin model (16.1 μ_B) is somewhat higher than that observed, but the situation is reasonable given the intragrid antiferromagnetic exchange. First-principles calculations involving this particular 39 electron spin model are too large for the average computer because of the extreme size of the matrix dimensions involved, and so attempts to model the exchange situation have not been carried out.

Variable temperature magnetic data for **4a**−**4c** are shown collectively in Figure 15 as plots of μ_{mol} as a function of temperature (black, green, red triangles, respectively). The general shapes of the profiles are very similar, with room temperature moments of ~14 μ_B in each case, followed by a drop to slightly varying minima (11−12 μ_B)

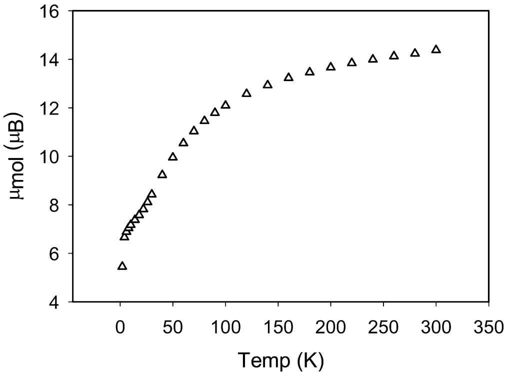

Figure 13. Variable temperature magnetic data for$[(2poap)_6Fe_9](ClO_4)_8{\cdot}18H_2O$ (**3**).

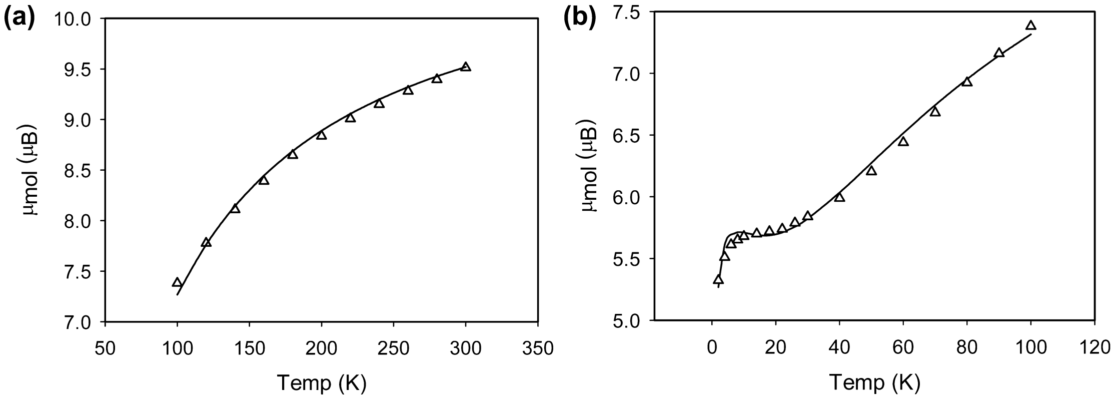

Figure 12. (a) Variable temperature magnetic data for $[(2poapz\text{-}H)_4Fe_4](NO_3)_6{\cdot}9H_2O$ (**2**) in the temperature range 100−300 K (see text for fitted parameters). (b) Variable temperature magnetic data for $[(2poapz\text{-}H)_4Fe_4](NO_3)_6{\cdot}9H_2O$ (**2**) in the temperature range 3−100 K (see text for fitted parameters).

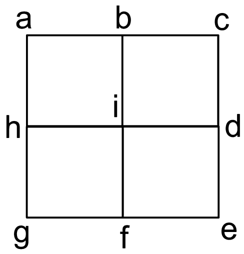

	a,c,e,g	b,d,f,h	i	ΣS′	Fe/4
1	5	4	5	9/2	
2	4	5	5	1/2	
3	5	4	4	8/2	
4	4	4	4	4/2	
5	5	5	5	5/2	
6	4,5,5,4	4,4,4,5	4	7/2	
7	5,5,5,5	4,0,4,0	5	17/2	0.50
8	5,5,5,5	2,2,2,2	5	17/2	0.50
9	5,5,5,5	4,0,4,2	5	15/2	0.625
10	5,5,5,5	4,2,4,2	5	13/2	0.75

Figure 14. Spin models for hypothetical [3 × 3] grids with mixtures of HS Fe(II) and HS Fe(III) centers.

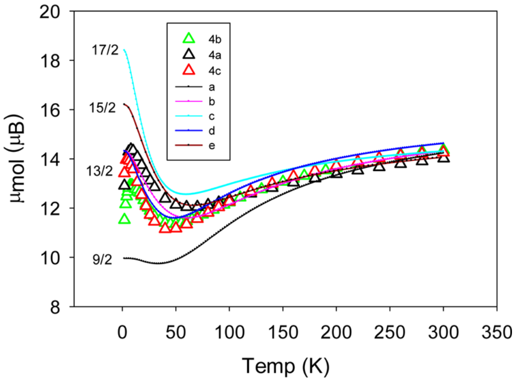

Figure 15. Variable temperature magnetic data for **4a**−**4c** as plots of μ_{mol} as a function of temperature (black, green, red triangles, respectively).

around 50−70 K and then a rise to maxima (13−15 μ_B) at ~10 K. The smooth drop from room temperature to ~60 K indicates intramolecular antiferromagnetic exchange, which would be expected as a result of the oxygen bridged grid structures. However, the minima and the rise below 60 K are indicative of the presence of a mixture of different spin states and a noncompensation of spins in the ground state, in what would be a ferrimagnetic system. The general overall similarity of the three profiles would be expected based on the structures. Magnetization data for **4a** versus field at 2 K (Figure 16) show that S_T ($S_T = \Sigma S_n$ in the antiferromagnetic limit) must have a high value ($M = 14.4$ Nβ at 5 T), but it does not become saturated at high field. Depending on an estimate of '*g*' it would be reasonable to assume that S_T is 13/2 or higher.

Given the evidence for ferrimagnetic behavior (*vide supra*), we can appeal to a spin exchange model which reflects a combination of spin sites with a noncompensated ground state spin arrangement. Various possible spin models have been considered and are summarized in Figure 14. Model 1 assumes $S = 5/2$ sites at the corners and center, and $S = 4/2$ sites at all side positions. The ground state in an antiferromagnetic limit is $S_T = 9/2$, clearly less than anticipated on the basis of the *M*/*H* data at 2 K for **4a**. In contrast, if the side and corner sites are reversed, the ground state is $S_T = 1/2$, which is clearly wrong. Given that the center and corner sites are $S = 5/2$, then raising the ground state spin can be effected only by reducing the number of electrons at the side sites. Cases 7−10 show how varying these spins affects S_T. With two sites vacant (i.e., $S = 0$), $S_T = 17/2$. Interestingly, this is the same as the isoelectronic situation where there are two electrons at each side site. Adding two more electrons lowers S_T to 15/2 and with two more S_T becomes 13/2. Given the *M*/*H* data for **4a** and the occupancy situation for the side sites in all three complexes from the X-ray data (~0.5−0.6), cases 7−10 seem the most realistic. Curie moments for these cases are 14.9 μ_B, 15.2 μ_B, and 15.4 μ_B, respectively. The room temperature moments for **4a**−**4c** (~14.0 μ_B) are close to all these examples, given the presence of intramolecular antiferromagnetic exchange. The averaged Fe occupancy at the side sites would be 0.50, 0.625, and 0.75, respectively.

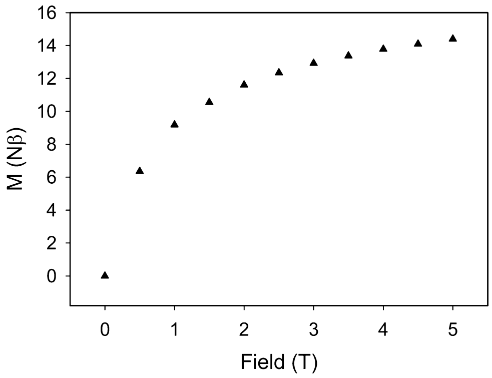

Figure 16. Magnetization data for **4a** versus field at 2 K.

$$H_{ex} = -J\{S_a \cdot S_b + S_b \cdot S_c + S_c \cdot S_d + S_d \cdot S_e + S_e \cdot S_f + S_f \cdot S_g + S_g \cdot S_h + S_h \cdot S_a + S_b \cdot S_i + S_d \cdot S_i + S_f \cdot S_i + S_h \cdot S_i\} \quad (3)$$

Given the extreme computational expense of dealing with the various spin models under consideration, and the "approximate" nature of these spin models, based on the structural data for **4a**−**4c**, no formal data fitting was attempted. Instead, theoretical magnetic profiles, based just on spin only exchange models, were calculated according to cases 1 and 7−10 (eq 3; Figure 14), assuming reasonable *g* and *J* values. These profiles were then compared with the experimental data for an overall approximate visual correspondence. For simplicity, only one exchange integral was assumed for the whole grid (eq 3; Figure 14; *J* applies to all Fe−Fe bridging connections). Plot 'a' shows the μ_{mol}/T profile for case 1, where all the side Fe2 sites are at unit occupancy ($S_T = 9/2$; Fe2/4 = 1.0; $g = 2.0$, $J = -15$ cm^{-1}). Clearly this is not a suitable model. At the other extreme, plot 'c' shows the profile based on cases 7 or 8 ($S_T = 17/2$; Fe2/4 = 0.5; $g = 2.05$, $J = -8$ cm^{-1}). Again, this is not a good match. Plots "b" and "d" (Figure 15) correspond to case 10 and are close matches ($S_T = 13/2$; Fe2/4 = 0.75; $g = 2.05$, $J = -15$ cm^{-1} and $g = 2.05$, $J = -12$ cm^{-1} respectively). Plot 'e' corresponds to case 9 ($S_T = 15/2$; Fe2/4 = 0.625; $g = 2.03$, $J = -14$ cm^{-1}), and although the low temperature match is not close, from 50 to 300 K the match is reasonable. Choosing the best model is problematic, given the complexity of the overall situation, but case 9 seems to be the most appropriate given all the variables. The fact that the low temperature match was not good can be rationalized in terms of some longer range exchange term within the grid, or a ZFS contribution, neither of which is incorporated into the spin only calculations.

[(Cl2poap)$_5$Fe$_6$](ClO$_4$)$_8$·20H$_2$O (5). Variable temperature magnetic data for **5** are shown in Figure 17 as a plot of μ_{mol} as a function of temperature. The moment per mole drops from 13.4 μ_B at 300 K to a plateau value of 9.2 μ_B with a more pronounced drop at ~8 K to a value of 8.2 μ_B at 2 K. The magnetic profile indicates the presence of intramolecular antiferromagnetic exchange, and the low temperature plateau indicates a nonzero spin ground state in a ferrimagnetic system. The structure indicates that three of the iron centers are HS Fe(III) (Fe2, Fe4, Fe6), and because of the isolated nature of the two trimetallic subunits in the open partial grid structure, the magnetic properties can be described by the sum of two independent trinuclear spin assemblies (eq 4; $S_1 = S_3 = S_5 = 4/2$; $S_2 = S_4 = S_6 = 5/2$). A reasonable fit to this model gave $g_{ave} = 2.24(2)$, $J = -12.5(9)$ cm^{-1},

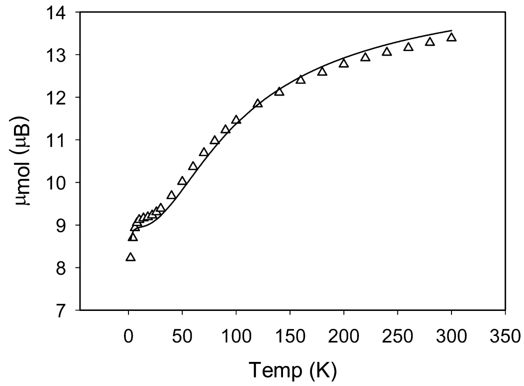

Figure 17. Variable temperature magnetic data for $[(\text{Cl2poap})_5\text{Fe}_6](\text{ClO}_4)_8\cdot 20\text{H}_2\text{O}$ (**5**) (see text for fitted parameters).

TIP = 500×10^{-6} cm^3 mol^{-1}, $\theta = -0.1$ K, $10^2R = 3.4$ (solid line Figure 17). Given the similarity in Fe−O−Fe bridge angles, the choice of one J value is reasonable.

$$H_{\text{ex}} = -J\{S_1{\cdot}S_2 + S_2{\cdot}S_3 + S_4{\cdot}S_5 + S_5{\cdot}S_6\} \tag{4}$$

CONCLUSIONS

A series of iron complexes with varying oxidation state combinations, involving three closely related tritopic bis-hydrazone ligands, is described, ranging from mononuclear to nonanuclear. Mixtures of Fe(II) and Fe(III) sites occur in the hexanuclear and nonanuclear complexes, despite starting with Fe(II), clearly related to the propensity of complexed iron(II) to undergo oxidation, but surprisingly a mixed valence tetranuclear complex was produced starting with Fe(III), implying Fe reduction. Structural and magnetic properties of the [2 × 2] tetranuclear, [3 + 3] hexanuclear, and one “formally” square [3 × 3] nonanuclear complex are described, and the magnetic coupling is quantified in terms of intramolecular antiferromagnetic exchange in what are ferrimagnetic systems with noncompensated ground state spins.

Three putative [3 × 3] Fe_9 square grid complexes were obtained by reacting Fe(II) with the ligand Cl2poap under slightly different conditions and found to be structurally almost identical, with the same space group and almost identical cell dimensions. However, there were inconsistencies in general between their structural and magnetic properties. Mössbauer data suggested a mixture of both high spin Fe(III) and Fe(II) sites, with the Fe(III) sites at the corners and the center, and Fe(II) sites at the sides of the grid. The initial structural refinements were based on unit occupancy at all sites including the side Fe(II) sites, but poor refinement statistics and large thermal ellipsoids at the side sites raised concerns about the validity of the structures. As a consequence of this situation, and the unusual and confusing magnetic properties of these complexes, the structures were refined again allowing the occupancies of just the side sites to vary. Remarkable improvements in refinement statistics were obtained, with unexpected occupancies of ∼0.5−0.6 at the side sites. This in turn led to an improved understanding of both the magnetic and Mössbauer properties of the grid systems, with the magnetic properties best described in terms of grids with ground state spins approximating $S_{\text{T}} = 15/2$. This is interpreted in terms of grids with fully metalated corner and center HS Fe(III) sites but incompletely metalated side Fe(II) sites. Such a situation is quite unusual and may be associated with kinetically based effects where the corner and center Fe(III) sites are occupied first, followed by the side Fe(II) sites.

Isolation of a grid based hexanuclear Fe(III)/Fe(II) partial grid, with the correct arrangement of ligands and metal ions on two parallel edges and missing the central metal triad, suggests that such a species may be formed in a penultimate full grid assembly step. The addition of the central Fe(III) would then occur via a mononuclear intermediate (e.g., similar to **1**), and finally the last two side Fe(II) sites would become filled. However, because the grid becomes effectively closed at this point, complete filling of these remaining sites is impeded, leading to grids with incomplete side site metalation.

ASSOCIATED CONTENT

Ⓢ Supporting Information

Crystal data for **4b** and **4c**, distances and angles for **4b** and **4c**, Mössbauer data for **4c**, structural figures for **4b** and **4c**, Mössbauer spectra for **4b**, variable temperature magnetic data for **5**, and a CIF file. This material is available free of charge via the Internet at http://pubs.acs.org.

AUTHOR INFORMATION

Corresponding Author

*E-mail: lk.thompson@mun.ca.

Notes

The authors declare no competing financial interest.

ACKNOWLEDGMENTS

We thank NSERC (Canada) for financial support for this study. Dr. Bob McDonald, University of Alberta, is acknowledged for data collection of **4b**, and Mr. David Miller, Memorial University, is acknowledged for the initial solution of **4b**.

REFERENCES

(1) Matthews, C. J.; Avery, K.; Xu, Z.; Thompson, L. K.; Zhao, L.; Miller, D. O.; Biradha, K.; Poirier, K.; Zaworotko, M. J.; Wilson, C.; Goeta, A. E.; Howard, J. A. K. *Inorg. Chem.* **1999**, *38*, 5266−5276.

(2) Thompson, L. K.; Matthews, C. J.; Zhao, L.; Xu, Z.; Miller, D. O.; Wilson, C.; Leech, M. A.; Howard, J. A. K.; Heath, S. L.; Whittaker, A. G.; Winpenny, R. E. P. *J. Solid State Chem.* **2001**, *159*, 308−320.

(3) (a) Zhao, L.; Matthews, C. J.; Thompson, L. K.; Heath, S. L. *Chem. Commun.* **2000**, 265. (b) Dawe, L. N.; Abedin, T. S. M.; Kelly, T. L.; Thompson, L. K.; Miller, D. O.; Zhao, L.; Wilson, C.; Leech, M. A.; Howard, J. A. K. *J. Mater. Chem.* **2006**, 2645−2659. (c) Dawe, L. N.; Shuvaev, K. V.; Thompson, L. K. *Inorg. Chem.* **2009**, *48*, 3323−3341. (d) Dawe, L. N.; Shuvaev, K. V.; Thompson, L. K. *Chem. Soc. Rev.* **2009**, *38*, 2334−2359 and references therein.

(4) Patroniak, V.; Baxter, P. N. W.; Lehn, L.-M.; Kubicki, M.; Nissinen, M.; Rissanen, K. *Eur. J. Inorg. Chem.* **2003**, 4001−4009.

(5) Baxter, P. N. W.; Lehn, J.-M.; Fischer, J.; Youinou, M. T. *Angew. Chem., Int. Ed.* **1994**, *33*, 2284−2287.

(6) Garcia, A. M.; Romero-Salguero, F. J.; Bassani, D. M.; Lehn, J.-M.; Baum, G.; Fenske, D. *Chem.—Eur. J.* **1999**, *5*, 1803−1808.

(7) Onions, S. T.; Frankin, A. M.; Horton, P. N.; Hursthouse, M. B.; Matthews, C. J. *Chem. Commun.* **2003**, 2864−2865.

(8) Baxter, P. N. W.; Lehn, J.-M.; Baum, G.; Fenske, D. *Chem.—Eur. J.* **2000**, *6*, 4510−4517.

(9) Dey, S. K.; Abedin, T. S. M.; Dawe, L. N.; Tandon, S. S.; Collins, J. L.; Thompson, L. K.; Postnikov, A. V.; Alam, M. S.; Müller, P. *Inorg. Chem.* **2007**, *46*, 7767−7781.

(10) Zhao, L.; Xu, Z.; Grove, H.; Milway, V. A.; Dawe, L. N.; Abedin, T. S. M.; Thompson, L. K.; Kelly, T. L.; Harvey, R. G.; Miller, D. O.; Weeks, L.; Shapter, J. G.; Pope, K. J. *Inorg. Chem.* **2004**, *43*, 3812−3824.

(11) Thompson, L. K.; Zhao, L.; Xu, Z.; Miller, D. O.; Reiff, W. M. *Inorg. Chem.* **2003**, *42*, 128−139.

(12) Milway, V. A.; Niel, V.; Abedin, T. S. M.; Xu, Z.; Thompson, L. K.; Grove, H.; Miller, D. O.; Parsons, S. R. *Inorg. Chem.* **2004**, *43*, 1874−1884.

(13) Milway, V. A.; Abedin, T. S. M.; Niel, V.; Kelly, T. L.; Dawe, L. N.; Dey, S. K.; Thompson, D. W.; Miller, D. O.; Alam, M. S.; Müller, P.; Thompson, L. K. *J. Chem. Soc., Dalton Trans.* **2006**, 2835−2851.

(14) Thompson, L. K.; Kelly, T. L.; Dawe, L. N.; Grove, H.; Lemaire, M. T.; Howard, J. A. K.; Spencer, E.; Matthews, C. J.; Onions, S. T.; Coles, S. J.; Horton, P. N.; Hursthouse, M. B.; Light, M. E. *Inorg. Chem.* **2004**, *43*, 7605−7616.

(15) Niel, V.; Milway, V. A.; Dawe, L. N.; Grove, H.; Tandon, S. S.; Abedin, T. S. M.; Kelly, T. L.; Spencer, E. C.; Howard, J. A. K.; Collins, J. L.; Miller, D. O.; Thompson, L. K. *Inorg. Chem.* **2008**, *47*, 176−189.

(16) Shapter, J. G.; Weeks, L.; Thompson, L. K.; Pope, K. J.; Xu, Z.; Johnston, M. R. *Smart Mater. Struct.* **2006**, *15*, S171−S177.

(17) Alam, M. S.; Strömsdörfer, S.; Dremov, V.; Müller, P.; Kortus, J.; Ruben, M.; Lehn, J.-M. *Angew. Chem., Int. Ed.* **2005**, *44*, 7896−7900.

(18) Alam, M. S.; Dremov, V.; Müller, P.; Postnikov, A. V.; Mal, S. S.; Hussain, F.; Kortz, U. *Inorg. Chem.* **2006**, *45*, 2866−2872.

(19) Saalfrank, R. W.; Scheurer, A.; Bernt, I.; Heinemann, F. W.; Postnikov, A. V.; Schünemann, V.; Trautwein, A. X.; Alam, M. S.; Rupp, H.; Müller, P. *J. Chem. Soc., Dalton Trans.* **2006**, 2865−2874.

(20) Ruben, M.; Lehn, J.-M.; Müller, P. *Chem. Soc. Rev.* **2006**, *35*, 1056−1067 and references therein.

(21) Sheldrick, G. M. *SAINTPLUS*, version 6.02; Bruker AXS: Madison, WI, 1997.

(22) SHELX: Sheldrick, G. M. *Acta Crystallogr., Sect. A* **2008**, *64*, 112−122.

(23) Sheldrick, G. M. *SADABS, Program for Absorption Correction*; University of Göttingen: Göttingen, Germany, 1998.

(24) SIR2008: Burla, M. C.; Caliandro, R.; Camalli, M.; Carrozzini, B.; Cascarano, G. L.; De Caro, L.; Giacovazzo, C.; Polidori, G.; Siliqi, D.; Spagna, R. *J. Appl. Crystallogr.* **2007**, *40*, 609−613.

(25) DIRDIF99: Beurskens, P. T.; Admiraal, G.; Beurskens, G.; Bosman, W. P.; de Gelder, R.; Israel, R.; Smits, J. M. M. *The DIRDIF-99 program system*, Technical Report of the Crystallography Laboratory, University of Nijmegen: Nijmegen, The Netherlands, 1999.

(26) Cromer, D. T.; Waber, J. T. Table 2.2 A. *International Tables for X-ray Crystallography*; The Kynoch Press: Birmingham, England, 1974; Vol. *IV*.

(27) Ibers, J. A.; Hamilton, W. C. *Acta Crystallogr.* **1964**, *17*, 781−782.

(28) Creagh, D. C.; McAuley, W. J. Table 4.2.6.8. *International Tables for Crystallography*; Wilson, A. J. C., Ed.; Kluwer Academic Publishers: Boston, 1992; Vol. *C* , pp 219−222.

(29) Creagh, D. C.; Hubbell, J. H. Table 4.2.4.3 in *International Tables for Crystallography*; Wilson, A. J. C., Ed.; Kluwer Academic Publishers: Boston, 1992; Vol. *C* , pp 200−206.

(30) *CrystalStructure 3.7.0: Crystal Structure Analysis Package*; Rigaku; Rigaku/MSC: The Woodlands, TX, 2000−2005.

(31) Watkin, D. J.; Prout, C. K.; Carruthers, J. R.; Betteridge, P. W. *CRYSTALS Issue 10*; Chemical Crystallography Laboratory: Oxford, UK,1996.

(32) OLEX2: Dolomanov, O. V.; Bourhis, L. J.; Gildea, R. J. *J. Appl. Crystallogr.* **2009**, *42*, 339−341.

(33) *SHELXTL*, version 5.1; Bruker AXS.: Madison, WI.

(34) PLATON: Spek, A. L. *J. Appl. Crystallogr.* **2003**, *36*, 7−13.

(35) Zhao, L.; Thompson, L. K.; Miller, D. O. *Polyhedron* **2001**, *20*, 1359−1367.

(36) (a) Palenik, G. J. *Inorg. Chem.* **1997**, *36*, 122. (b) O'Keeffe, M.; Brese, N. E. *J. Am. Chem. Soc.* **1991**, *113*, 3226−3229.

(37) Gütlich, P.; Link, R.; Trautwein, A. X. *Mössbauer Spectropscopy and Transition Metal Chemistry*; Springer: Berlin, 1978.

(38) Reger, D. L.; Little, C. A.; Rheingold, A. L.; Lam, M.; Concolino, T.; Mohan, A.; Long, G. L. *Inorg. Chem.* **2000**, *39*, 4674−4675.

(39) MAGMUN4.1/OW01.exe is available as a combined package free of charge from the authors (http://www.ucs.mun.ca/~lthomp/magmun). It was developed by Dr. Z. Xu (Memorial University) and OW01.exe by Pr. Dr. O. Waldmann. Source codes are not distributed. The origin of the programme should be quoted. Spin state and energy calculations appropriate to a particular exchange Hamiltonian are calculated within the software, including the appropriate non-linear regressions using experimental variable temperature magnetic data.